Time-domain ultrasound diffraction tomography

T. Douglas Mast,[1] Feng Lin,[2] and Robert C. Waag[2,3]

[1]Applied Research Laboratory, The Pennsylvania State University, University Park, PA 16802
[2]Dept. of Electrical Engineering, University of Rochester, Rochester, NY 14627
[3]Dept. of Radiology, University of Rochester, Rochester, NY 14642

Abstract— **A quantitative ultrasonic imaging method employing time-domain scattering data is presented. This method provides tomographic images of medium properties such as the sound speed contrast; these images are equivalent to multiple-frequency filtered-backpropagation reconstructions using all frequencies within the bandwidth of the incident pulse employed. However, image synthesis is performed directly in the time domain using coherent combination of farfield scattered pressure waveforms, delayed and summed to numerically focus on the unknown medium. The time-domain method is more efficient than multiple-frequency diffraction tomography methods, and can, in some cases, be more efficient than single-frequency diffraction tomography. Example reconstructions, obtained using synthetic data for two-dimensional and three-dimensional scattering of wideband pulses as well as measured scattering data from a 2048-element ring transducer, show that the time-domain reconstruction method provides image quality superior to single-frequency reconstructions for objects of size and contrast relevant to medical imaging problems such as ultrasonic mammography. The present method is closely related to existing synthetic-aperture imaging methods such as those employed in clinical ultrasound scanners. Thus, the new method can be extended to incorporate available image-enhancement techniques such as time-gain compensation to correct for medium absorption and aberration correction methods to reduce error associated with weak scattering approximations.**

I. Introduction

Quantitative imaging of tissue properties is a potentially useful technique for diagnosis of cancer and other disease. Inverse scattering methods such as diffraction tomography can provide quantitative reconstruction of tissue properties including sound speed, density, and absorption. However, although previous inverse scattering methods have achieved high resolution and quantitative accuracy, such methods have not yet been incorporated into commercially successful medical ultrasound imaging systems. Previous methods of diffraction tomography have usually been based on single-frequency scattering, while current diagnostic ultrasound scanners employ wideband time-domain signals. The use of wideband information in image reconstruction is known to provide increased point and contrast resolution, both of which are important for medical diagnosis.

Relatively few previous workers have investigated direct use of wideband scattering data for inverse scattering methods analogous to single-frequency diffraction tomography. A review of several approaches is given in Ref. [1], including linear and nonlinear diffraction tomography methods using scattering data for a number of discrete frequencies [2]–[4], a direct (but not completely general) time-domain reconstruction algorithm [5], and an extension of the eigenfunction method from Ref. [4] to use the full bandwidth of the incident pulse waveform [6].

Recently, a new approach to wideband quantitative imaging has been offered: a time-domain inverse scattering method that overcomes some of the limitations of previous frequency-domain and time-domain quantitative imaging methods [1]. In this paper, the new time-domain diffraction tomography algorithm is briefly reviewed. The capabilities of the method are demonstrated using simulated reconstructions of two-dimensional and three-dimensional scatterers. The practical capability of the method for ultrasonic mammography is then illustrated by reconstructions of tissue-mimicking phantoms from scattering data measured by a 2.5 MHz, 2048-element ring transducer.

II. Theory

A new time-domain inverse scattering algorithm, applicable to quantitative imaging of tissue and other inhomogeneous media, is derived in Ref. [1] and summarized briefly below. The medium is modeled as a fluid medium defined by the sound speed contrast function $\gamma(\mathbf{r}) = c_0^2/c(\mathbf{r})^2 - 1$, where c_0 is a background sound speed and $c(\mathbf{r})$ is the spatially-dependent sound speed defined at all points $\mathbf{r}$. For the scope of the present paper, the medium is assumed to have constant density, no absorption, and weak scattering characteristics; extensions to the reconstruction algorithm that overcome these limiting assumptions are discussed in Ref. [1].

The medium is subjected to a pulsatile plane wave of the form $p_{\text{inc}}(\mathbf{r}, \boldsymbol{\alpha}, t) = f(t - \mathbf{r} \cdot \boldsymbol{\alpha}/c_0)$, where $\boldsymbol{\alpha}$ is a unit vector in the direction of propagation, f is the time-domain waveform, and c_0 is the background sound speed. The scattered wavefield $p_s(\boldsymbol{\theta}, \boldsymbol{\alpha}, t)$ is measured at a fixed radius R in the farfield, where $\boldsymbol{\theta}$ corresponds to the direction unit vector of a receiving transducer element. (Alternatively, if scattering measurements are made in the nearfield, the farfield acoustic pressure can be computed using exact transforms that represent propagation through a homogeneous medium [2].) The farfield scattered pressure, when specified for all incident-wave directions $\boldsymbol{\alpha}$, measurement directions $\boldsymbol{\theta}$, and times t, comprises the data set to be used for reconstruction of the unknown medium. The inverse scattering problem is to reconstruct the unknown medium contrast $\gamma(\mathbf{r})$ using the scattered field $\hat{p}_s(\boldsymbol{\theta}, \boldsymbol{\alpha}, \omega)$ measured at a fixed radius R.

The starting point for the present time-domain inverse scattering method is single-frequency filtered backpropagation [2], [7], [8]. Under the assumption of weak scattering, such that the Born approximation holds, the solution to the single-frequency inverse scattering problem is given by the formula

$$\gamma_B(\mathbf{r}, \omega) = \frac{\hat{\mu}(\omega)\, e^{-ikR}}{\hat{f}(\omega)} \iint \Phi(\boldsymbol{\theta}, \boldsymbol{\alpha})\, \hat{p}_s(\boldsymbol{\theta}, \boldsymbol{\alpha}, \omega) \times e^{ik(\boldsymbol{\theta} - \boldsymbol{\alpha}) \cdot \mathbf{r}}\, dS_\alpha\, dS_\theta, \text{ where} \quad (1)$$

0-7803-5722-1/99/$10.00

$$\hat{\mu}(\omega) = \sqrt{\frac{kR}{8i\pi^3}},\ \Phi(\boldsymbol{\theta},\boldsymbol{\alpha}) = |\sin(\theta-\alpha)| \text{ in 2D, and}$$

$$\hat{\mu}(\omega) = \frac{kR}{4\pi^3},\ \Phi(\boldsymbol{\theta},\boldsymbol{\alpha}) = |\boldsymbol{\theta}-\boldsymbol{\alpha}| \text{ in 3D.} \quad (2)$$

Each surface integral in Eq. (1) is performed over the entire measurement circle for the 2D case and over the entire measurement sphere for the 3D case. Equation (1) provides an exact solution to the linearized inverse scattering problem for a single frequency component of the scattered wavefield $p_s(\boldsymbol{\theta},\boldsymbol{\alpha},t)$. The resulting reconstruction, $\gamma_B(\mathbf{r},\omega)$, has spatial frequency content limited by the "Ewald sphere" of radius $2k$ in wavespace [9].

To improve upon the single-frequency formulas specified by Eq. (1), one can extend the spatial-frequency content of reconstructions by exploiting wideband scattering information. The method outlined here synthesizes a "multiple-frequency" reconstruction $\gamma_M(\mathbf{r})$ by formally integrating single-frequency reconstructions $\gamma_B(\mathbf{r},\omega)$ over a range of frequencies ω. A general formula for this approach is

$$\gamma_M(\mathbf{r}) = \frac{\int_0^\infty \hat{g}(\omega)\,\gamma_B(\mathbf{r},\omega)\,d\omega}{\int_0^\infty \hat{g}(\omega)\,d\omega,} \quad (3)$$

where $\hat{g}(\omega)$ is an appropriate frequency-dependent weighting function. In practice, the weighting function $\hat{g}(\omega)$ is chosen to be bandlimited because (for a given set of physical scattering measurements) the frequency-dependent contrast $\gamma_B(\mathbf{r},\omega)$ can only be reliably reconstructed for a finite range of frequencies ω associated with the spectra of the incident waves employed. Thus, the integrands in Eq. (3) are nonzero only over the support of $\hat{g}(\omega)$ and the corresponding integrals are finite.

If the frequency weighting function is now specified to incorporate the incident-pulse spectrum as well as the frequency- and dimension-dependent coefficient $\hat{\mu}(\omega)$, such that $g(\omega) = \hat{f}(\omega)/\hat{\mu}(\omega)$, Eq. (3) reduces to the form [1]

$$\gamma_M(\mathbf{r}) = \frac{1}{N}\iint \Phi(\boldsymbol{\theta},\boldsymbol{\alpha})\left(p_s(\boldsymbol{\theta},\alpha,\tau)\right.$$
$$\left. + i\,\mathbf{H}^{-1}\left[p_s(\boldsymbol{\theta},\alpha,\tau)\right]\right)\,dS_\alpha\,dS_\theta, \text{ where} \quad (4)$$

$$\tau = R/c_0 + \frac{(\boldsymbol{\alpha}-\boldsymbol{\theta})\cdot\mathbf{r}}{c_0},\ N = 2\int_0^\infty \hat{g}(\omega)\,d\omega,$$

and $\mathbf{H}^{-1}$ is the inverse Hilbert transform, also known as a quadrature filter.

Equation (4) is notable in several respects. First, it provides a linearized reconstruction that employs scattering information from the entire signal bandwidth without any frequency decomposition of the scattered wavefield. Second, the delay term τ corresponds exactly to the delay required to construct a focus at the point $\mathbf{r}$ by delaying and summing the scattered wavefield $p_s(\boldsymbol{\theta},\boldsymbol{\alpha},t)$ for all measurement directions $\boldsymbol{\theta}$ and incident-wave directions $\boldsymbol{\alpha}$. Thus, the time-domain reconstruction formula given by Eq. (4) can be regarded as a quantitative generalization of confocal time-domain synthetic aperture imaging (*e.g.*, the "gold standard" beamformer of Ref. [10]), in which signals are synthetically delayed and summed for each transmit/receive pair to focus at the image point of interest.

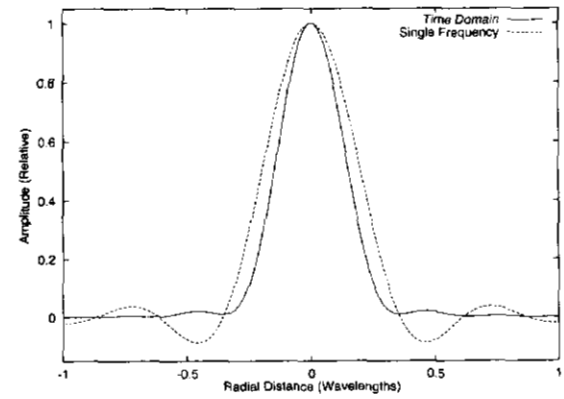

Fig. 1. Point-spread function for three-dimensional time-domain and single-frequency diffraction tomography methods. The vertical scale corresponds to the relative amplitude of the reconstructed contrast $\gamma(\mathbf{r})$, while the horizontal scale corresponds to number of wavelengths at the center frequency.

III. Simulations

Below, the time-domain diffraction tomography method of Ref. [1] is illustrated using results of simulation tests with 2D and 3D synthetic data. The synthetic scattering data employed were obtained using a Born approximation method for point scatterers and 3D slabs, and a k-space method [11] for arbitrary 2D inhomogeneous media. Additional results, presented in Ref. [1], show reconstructions performed using using exact time-domain solutions for scattering from compressible cylinders as well as reconstructions from limited-aperture data. The time-domain waveform employed for all the simulations reported here was $f(t) = \cos(2\pi f_0 t)\,e^{-t^2/(2\sigma^2)}$, with $f_0 = 2.5$ MHz and $\sigma = 0.25$ μs, so that the -6 dB bandwidth of the signal was 1.5 MHz. These parameters correspond closely to those of the ring transducer used in the measurements reported in the next section.

The time-domain imaging method was directly implemented using Eq. (4), evaluated using straightforward numerical integration over all incident-wave and measurement directions employed. The synthetic data employed was sampled at rates slightly larger than the Nyquist frequency. Before evaluation of the argument τ for each signal, the time-domain waveforms were Fourier interpolated at a sampling rate of 16 times the original rate. This resampling, as well as the inverse Hilbert transform from Eq. (4), were performed by FFT. Values of the pressure signals at the time τ were then determined using linear interpolation between samples of the resampled waveforms.

A three-dimensional point-spread function (PSF) for the present time-domain diffraction tomography method is illustrated in Fig. 1. The PSF was determined by reconstructing an ideal point scatterer located at the origin. The time-domain reconstruction shows a dramatic improvement over the single-frequency reconstruction, with significant increases in both the point resolution (PSF width at half-maximum reduced by 27%) and contrast resolution (first sidelobe reduced by 13 dB and second sidelobe reduced by 18 dB).

Reconstructions for several arbitrary scattering objects are shown in Fig. 2. All of these reconstructions were performed using synthetic data produced by the k-space method described in Ref. [11]. Synthetic scattering data were computed for 64 incident-wave directions and 256 measure-

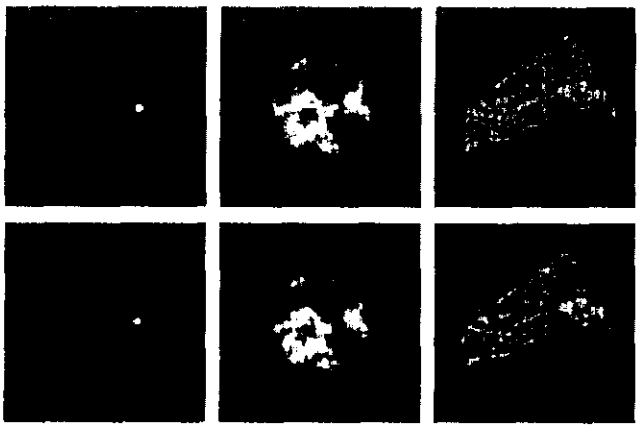

Fig. 2. Time-domain reconstructions from full-wave synthetic data for three arbitrary scattering objects. The upper row shows the contrast function γ for each object, while the lower row shows the real part of the reconstructed contrast γ_M. Each panel shows a reconstruction area of 5 mm × 5 mm using a linear bipolar gray scale. Left to right: (a) Cylinder, radius 2.5 mm, with an internal cylinder of radius 0.2 mm. (b) Cylinder, radius 2.5 mm, with random internal structure. (c) Tissue structure, with variable sound speed and density, from a chest wall cross section.

ment directions in each case. The first panel shows a reconstruction of a cylinder of radius 2.5 mm and contrast $\gamma = -0.0295$ with an internal cylinder of radius 0.2 mm and contrast $\gamma = 0.0632$. These contrast values correspond, based on tissue parameters given in Ref. [12], to the sound-speed contrasts of human skeletal muscle for the outer cylinder and of human fat for the inner cylinder. The second panel shows a reconstruction of a 2.5 mm-radius cylinder with random internal structure. The third reconstruction shown employed a portion of a chest wall tissue map from Ref. [13]. In this case, the synthetic data was obtained using a tissue model that incorporates both sound speed and density variations, so that the actual reconstructed quantity is slightly different from γ_M [1]. In Fig. 2(c), black denotes connective tissue, dark gray denotes muscle, and light gray denotes fat.

The real part of each reconstruction in Fig. 2 shows good image quality, with high resolution and very little evidence of artifacts. Particularly notable is the accurately detailed imaging of internal structure for the random cylinder and the chest wall cross section. As discussed in Ref. [1], the density variations present in the chest wall cross section have not greatly affected the image appearance; there is, however, a slight edge enhancement at boundaries between tissue regions. Also notable is the nearly-complete absence of any artifacts outside the scatterer in each case; this result indicates that high contrast resolution has been achieved.

Three-dimensional reconstructions of a homogeneous slab with sound speed contrast $\gamma = 0.01$ and dimensions 1 mm × 2 mm × 3 mm, are shown in Fig. 3. Synthetic data was computed using a weak scattering approximation for 288 incident-wave directions and 1152 measurement directions, each evenly spaced in the angles Φ and Θ. Isosurface renderings of the real part of the reconstructed γ_M are shown for the surfaces $\gamma_M = 0.0025$. Consistent with the point-spread function shown in Fig. 1, the time-domain reconstruction is much more accurate than the single-frequency reconstruction. While the single-frequency reconstruction shows an erroneously rippled surface, the time-domain reconstruction is smooth. The time-domain reconstruction is nearly identical to the original object except for some round-

Fig. 3. Three-dimensional reconstructions of a uniform slab with contrast $\gamma = 0.01$. Each reconstruction shows an isosurface rendering of the surface $\gamma_M = 0.0025$. Left: single-frequency reconstruction. Right: time-domain reconstruction.

Fig. 4. Reconstructions of three phantoms from measured scattering data. Each panel shows an area of 9 mm × 9 mm using a bipolar logarithmic scale with a 30 dB dynamic range. Left to right: (a) Homogeneous agar cylinder. (b) Agar with glass spheres. (c) Agar with glass spheres and three nylon filaments.

ing of the sharp edges due to the limited high-frequency content of the signal employed. The length scale of the rounded edges is on the order of one-half the wavelength of the highest frequency in the pulse, *i.e.*, about 0.2 mm for the −6 dB cutoff of 3.25 MHz. Notable is that the time-domain method was more efficient than the single-frequency method in this case; the total CPU time required on a 233 MHz Pentium II processor was 100.0 CPU min for the time-domain method and 233.4 CPU min for the single-frequency method (both computations included solution of the applicable linearized forward problem as well as the inverse problem). This gain in efficiency was possible because the greatest computational expense occurred in the "backpropagation" of the signals, which required evaluation of complex exponentials for the single-frequency method, but only linear interpolation of the oversampled farfield pressure waveforms for the time-domain method.

IV. Measurements

The practical capability of the time-domain diffraction tomography method to image tissue-like media has been tested using measured scattering data for three tissue-mimicking phantoms, each of diameter 6 mm. Details of the phantom construction and measurement procedure are given in Ref. [6] and briefly summarized here. The phantoms are primarily composed of agar (nominal sound speed 1510 m/s); one is homogeneous, another contains tiny (subresolution), randomly distributed glass beads, and a third contains three nylon filaments as well as glass beads. Measurements were made using a ring transducer system [14] that consists of 2048 elements, each of which can be used independently as a transmitter or receiver. This fixed transducer configuration avoids signal degradation from phase jitter and excessive scanning time associated with moving transducers. The control electronics associated with the ring transducer provide the capability to program arbitrary transmit waveforms. The element pitch is 0.23 mm, less than one half of the wavelength at the nominal center frequency of 2.5 MHz.

Spatially-limited plane wave pulses were transmitted

from 128 positions equally spaced around the ring. To construct the spatially-limited plane waves, a 4 mm-width cosine rolloff was added to each side of a 10 mm-width uniform central region to provide a smooth transition in amplitude and reduce wavefront spreading. A backpropagation method [15] was then used to obtain the transmit waveforms that produced the desired incident wave.

The incident field (without the scattering object) and the total field (with the scattering object) were measured around the ring for each incident view. To compensate for sound speed changes due to water temperature variations, the background sound speed was tracked using a probe beam during the measurement of both the incident and total fields. The sound speed in the background was estimated from knowledge of the arrival time and the travel distance of the probe beam, which was a spatially limited plane wave directed to the side of the phantom. The resulting speed estimate was used to equalize the time scale of all waveforms. A temperature-compensated incident field $p_i(\theta, \alpha, t)$ was subtracted from the total field $p(\theta, \alpha, t)$ to obtain the scattered field $p_s(\alpha, \theta, t)$. Finally, wavefields were extrapolated to 128 measurement positions at a radius of 7500 mm by an exact spatio-temporal transformation [2], [6].

Far-field scattered waveforms for each incident-wave direction were further processed by a deconvolution operation [1] that compensated for transducer-dependent variations in the incident pulse. The result for each incident-wave direction was an estimate of the scattered farfield pressure associated with an ideal incident pulse of the form $f(t) = \cos(2\pi f_0 t)\, e^{-t^2/(2\sigma^2)}$, with $f_0 = 2.25$ MHz and $\sigma = 0.25$ μs. The preprocessed data $p_s(\theta, \alpha, t)$ were then inverted using numerical integration of Eq. (4). The inversion procedure was the same as for the simulations described above, except that the initial sampling rate was 20 MHz and that signals were oversampled to 80 MHz by Fourier interpolation.

Reconstructions for the three phantoms are shown in Fig. 4. Each panel shows good reconstruction quality with a uniform background and high point and contrast resolution as well as quantitative accuracy (similar reconstructions, obtained using an eigenfunction-based inverse scattering method, are presented in Ref. [6]). The subresolution glass spheres do not cause speckle as in pulse-echo B-scan imaging, but instead appear as slight local variations in contrast consistent with weak point scatterers. Both nylon filaments and glass spheres appear dark because higher sound speed corresponds to negative contrast γ as defined above. In panel (c), reconstructions of the nylon wires show slight sidelobe artifacts; these artifacts could be removed by careful choice of an optimal pulse $f(t)$ in the preprocessing of the scattered field [6].

V. Conclusions

A new method for time-domain ultrasound diffraction tomography has been presented and validated using synthetic and measured scattering data. The method provides quantitative images of sound speed variations in unknown media. These reconstructions are equivalent to multiple-frequency reconstructions using filtered backpropagation, but can be obtained with much greater efficiency. The time-domain reconstruction algorithm has been derived as a simple filtered delay-and-sum operation, closely related to time-domain confocal synthetic aperture imaging, so that it can be considered a generalization of imaging algorithms employed in current clinical instruments. The simplicity of the imaging algorithm allows straightforward addition of features such as time-gain compensation and aberration correction.

Numerical results obtained using synthetic and measured data show that the time-domain method can yield significantly higher image quality (and, in some cases, also greater efficiency) than single-frequency diffraction tomography. Quantitative reconstructions, obtained using signal parameters comparable to those for present-day clinical instruments, show accurate imaging of objects with simple deterministic structure, random internal structure, and structure based on a cross-sectional tissue model. Reconstructions of tissue-mimicking phantoms suggest that the method will be useful for diagnostic imaging problems such as the detection and characterization of lesions in ultrasonic mammography.

Acknowledgments

This research was funded by the Breast Cancer Research Program of the U.S. Army Medical Research and Materiel Command, under Grant No. DAMD17-98-1-8141 (TDM), and by NIH Grants DK 45533, HL 50855, and CA 74050, DARPA Grant N00014-96-0749, and the University of Rochester Diagnostic Ultrasound Research Laboratory Industrial Associates (FL and RCW).

References

[1] T. D. Mast, "Wideband quantitative ultrasonic imaging by time-domain diffraction tomography," to appear in J. Acoust. Soc. Am. (1999).

[2] A. Witten, J. Tuggle, and R. C. Waag, "A practical approach to ultrasonic imaging using diffraction tomography," J. Acoust. Soc. Am. **83**, 1645–1652 (1988).

[3] T. J. Cavicchi and W. D. O'Brien, "Numerical study of higher-order diffraction tomography via the sinc basis moment method," Ultrasonic Imaging **11**, 42–74 (1989).

[4] T. D. Mast, A. I. Nachman, and R. C. Waag, "Focusing and imaging using eigenfunctions of the scattering operator," *J. Acoust. Soc. Am.* **102**, 715–725 (1997).

[5] V. A. Burov and O. D. Rumyantseva, "Linearized inverse problem of scattering in monochromatic and pulse modes," Acoustical Physics **40**, 34–42 (1996).

[6] F. Lin, A. I. Nachman, and R. C. Waag, "Quantitative imaging using a time-domain eigenfunction method," submitted to J. Acoust. Soc. Am. (1999).

[7] A. J. Devaney, "A filtered backpropagation algorithm for diffraction tomography," Ultrason. Imag. **4**, 336–350 (1982).

[8] G. Beylkin, "The fundamental identity for iterated spherical means and the inversion formula for diffraction tomography and inverse scattering," J. Math. Phys. **24**, 1399–1400 (1982).

[9] E. Wolf, "Three-dimensional structure determination of semi-transparent objects from holographic data," Optics Comm. **1**, 153–156 (1969).

[10] K. E. Thomenius, "Evolution of ultrasound beamformers," Proc. IEEE Ultrason. Symp. **2**, 1615–1622 (1996).

[11] L. P. Souriau, T. D. Mast, D.-L. Liu, M. Tabei, A. I. Nachman, and R. C. Waag, "A k-space method for large-scale models of wave propagation in tissue," submitted to *IEEE Trans. Ultrason. Ferrolectr. Freq. Contr.* (1999).

[12] T. D. Mast, L. M. Hinkelman, M. J. Orr, V. W. Sparrow, and R. C. Waag, "Simulation of ultrasonic pulse propagation through the abdominal wall," J. Acoust. Soc. Am. **102**, 1177–1190 (1997).

[13] T. D. Mast, L. M. Hinkelman, M. J. Orr, and R. C. Waag, "Simulation of ultrasonic pulse propagation, distortion, and attenuation in the human chest wall," submitted to J. Acoust. Soc. Am. (1999).

[14] T. T. Jansson, T. D. Mast, and R. C. Waag, "Measurements of differential scattering cross section using a ring transducer," J. Acoust. Soc. Am. **103**, 3169–3179 (1998).

[15] D.-L. Liu and R. C. Waag, "Propagation and backpropagation for ultrasonic wavefront design," IEEE Trans. Ultrason., Ferroelect., Freq. Contr. **44**, 1–13 (1997).